Bubble-Propelled Plasmon-Reinforced Pt-$ZnIn_2S_4$ Micromotors for Stirring-Free Photocatalytic Water Purification

Mengge Yuan, Mengqin Gong, Hai Huang,Yu Zhao, Yulong Ying*, and Sheng Wang*

School of Materials Science and Engineering, Zhejiang Sci-Tech University, Hangzhou, 310018, P. R. China.

E-mail: yingyulong@zstu.edu.cn; wangsheng571@hotmail.com

*Corresponding author

Supporting Information

Contents

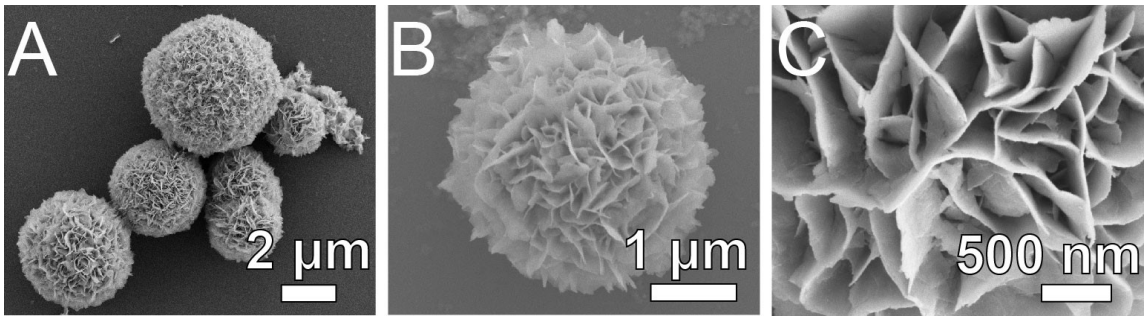

Figure S1. SEM images of the pristine ZIS microspheres at different magnifications.

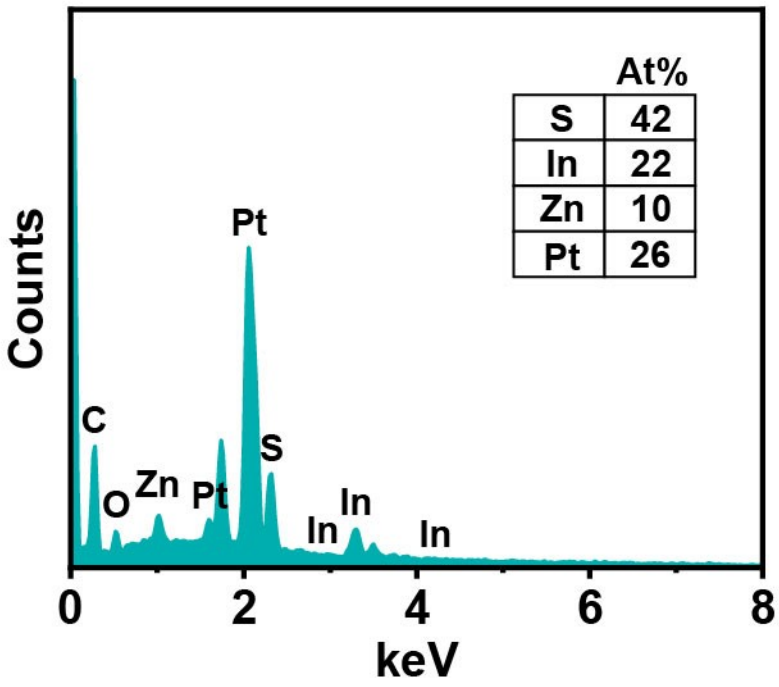

Figure S2. EDS spectrum of the Pt-ZIS micromotors.

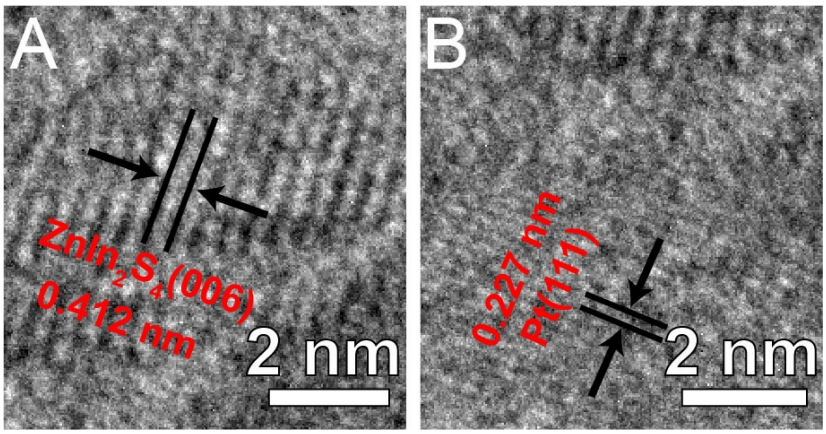

Figure S3. HRTEM images illustrate the presence of (A) ZIS and (B) Pt NPs on the Pt-ZIS micromotors.

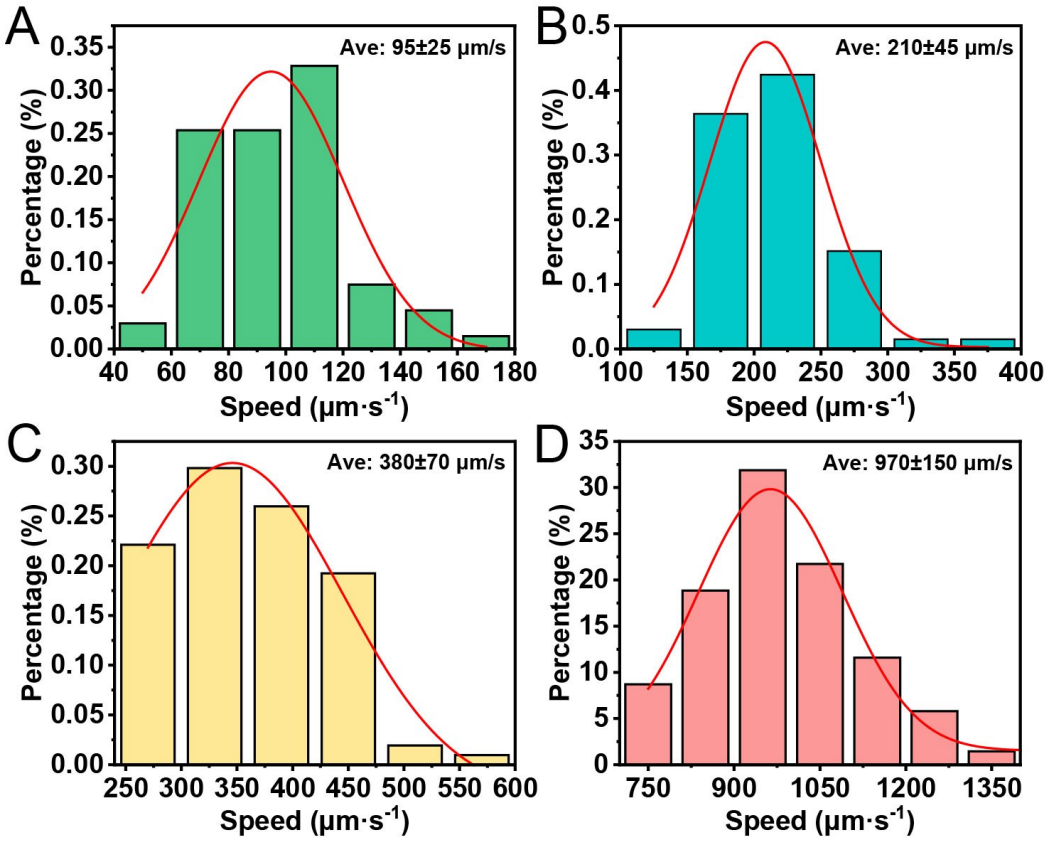

Figure S4. Statistical velocity distribution of the Pt-ZIS micromotors in (A) 1 wt% H_2O_2, (B) 3 wt% H_2O_2, (C) 5 wt% H_2O_2, (D) 10 wt% H_2O_2 aqueous solution (1 wt% SDS). The results were calculated from 50 representative micromotors under different conditions.

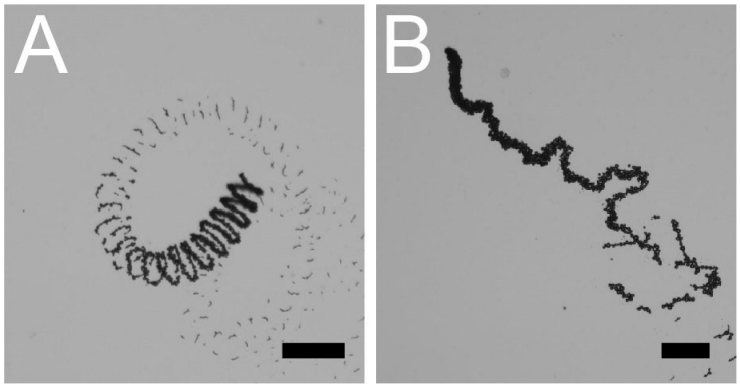

Figure S5. Motion characterization of the Pt-ZIS micromotors. (A) Present spiral and (B) curve propulsion (5 wt% H_2O_2). Scale bar, 200 μm.

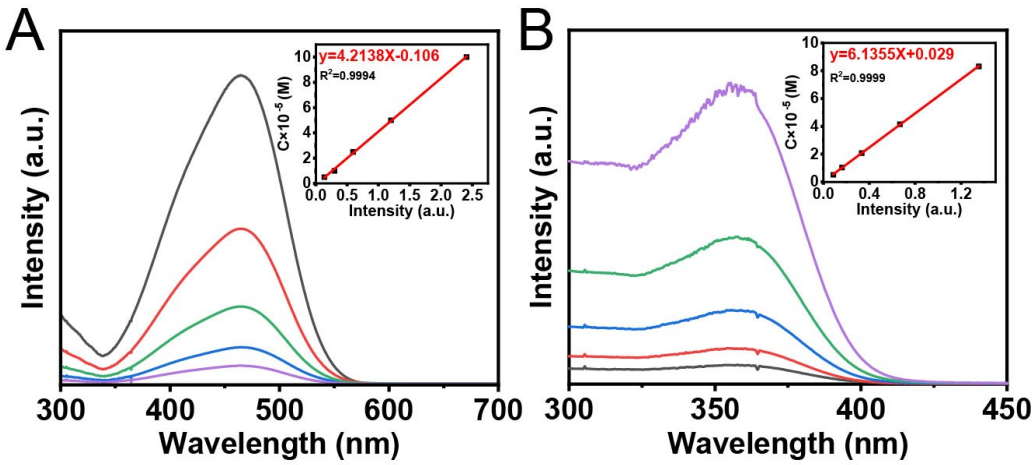

Finger S6. The UV-Vis absorption spectra of (A) MO and (B) TCH aqueous solution at different concentrations. The insets are the corresponding standard calibrated curve of absorbance-concentration.

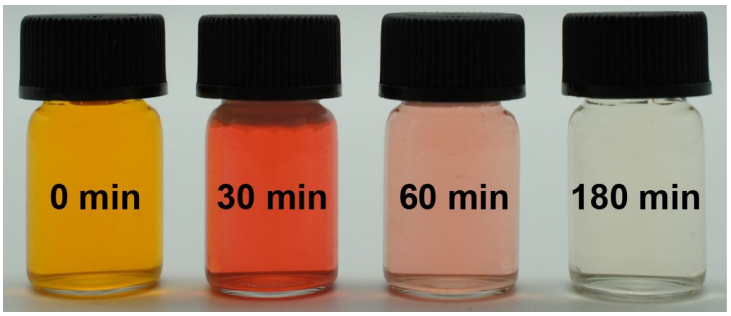

Figure S7. Time-dependent digital photographs of MO aqueous solution treated by Pt-ZIS micromotors at the best condition (8-Pt-ZIS||H_2O_2+Vis). The color change from orange to red is due to the addition of H_2O_2.

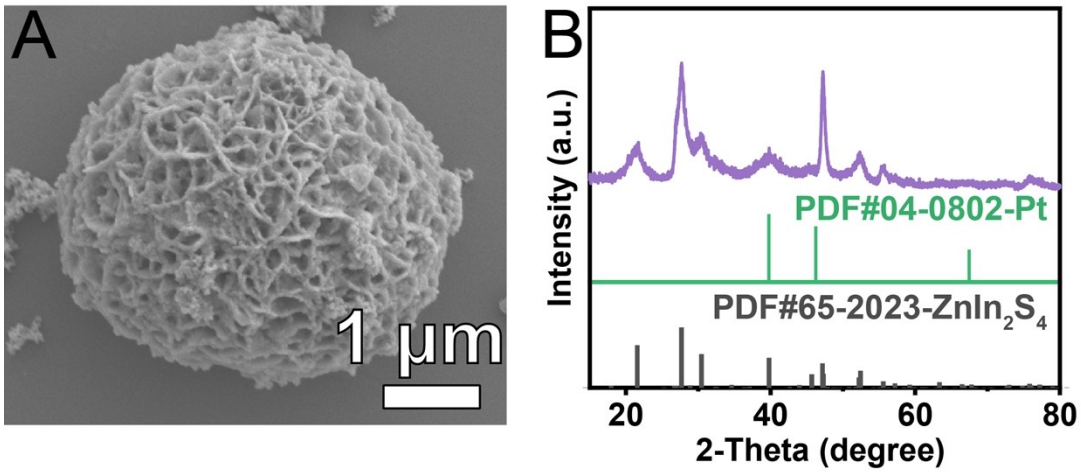

Figure S8. (A) SEM images and (B) XRD patterns of Pt-ZIS micromotors after three cycles of MO degradation test.

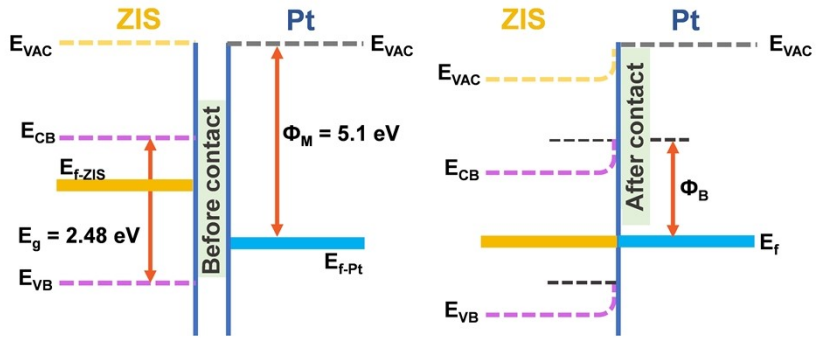

Figure S9. Band alignment structure for Pt and ZIS before contact and after contact. Φ_M — work function of Pt, Φ_B — Schottky barrier, E_{VB} — Valance band energy E_{CB} — Conduction band energy, E_f — Fermi level energy, E_{vac} — Vacuum energy level.

The loading Pt NPs on the surface of ZIS can effectively reduce the charge recombination at interfaces and surfaces. The relationship between the absolute electron potential of an electrode (E_{abs}) and the standard electrode potential (E^{θ}) is expressed as follows:[1]

$$E_{abs} = -E^{\theta} - 4.44 \qquad \text{(at 298 K)} \qquad (1)$$

According to the conversion formula, the valence band and conduction band potential of ZIS are equivalent to -6.04 eV and -3.56 eV in the vacuum level (E_{vac}). Since the Fermi level of platinum (E_f = -5.1 eV)[2] is lower and more negative to the conduction band of ZIS, the excited electrons move more easily from the CB of the semiconductor to the Fermi level of the Pt after contact. The as-built Schottky barrier (Φ_B) at a metal-semiconductor junction inhibits the exciton recombination process.[3]

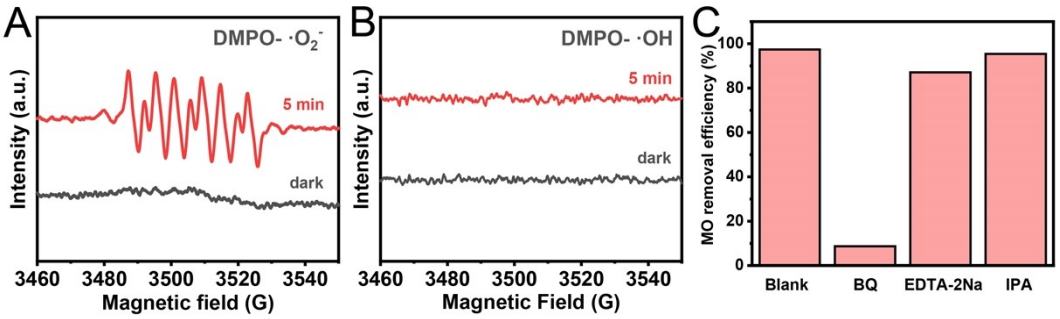

Figure S10. EPR spectra of (A) DMPO−•O_2^- and (B) DMPO−•OH adducts in the photocatalytic systems of Pt-ZIS after 5 min irradiation of the visible light, (C) MO photodegradation efficiencies with different scavengers. (BQ: 1 mM, EDTA-2Na: 1 mM, and IPA: 1 wt%)

Table S1. The current techniques in the preparation of bubble-propelled micromotors

Bubble-Propelled Micromotors	Preparation Method	Condition and Instruments	Ref.
Pt-$ZnIn_2S_4$ Micromotors	UV photoreduction deposition method	Reduction of $H_2PtCl_6 \cdot 6H_2O$ by ultraviolet light (XPA series photochemical reactor)	This work
S-CuFC/Ni/Pt Janus micromotors	Physical deposition	S-CuFC particles were evenly dispersed across the PVP layer to form a monolayer, Pt (50 nm) is deposited on top of it (E-beam evaporator (Korea Vacuum Tech) and sputter (A&E Korea))	S4
Pt/TiO_2 Microrobots	High vacuum sputtering coating method	Pt metal was deposited on TiO_2 particles in a high vacuum condition (Leica EM ACE600 sputter coater)	S5
TiO_2-Pt Micromotor	Physical sputtering method	A single layer of TiO_2 particles was dropped on the slide, and a platinum layer was sputtered on top (HHV-TF500 E-beam evaporator)	S6
SiO_2-Pt_{np} Janus Microspheres	Physical sputtering method	Sputtering Pt of 10 nm on a monolayer of SiO_2 spheres in a chamber prefilled with Ar, operating at a vacuum level of 6.77×10^{-3} Torr; (Leica EM ACE600 sputter coater)	S7
ZnO/Pt Micromotors	Physical vapor deposition method	Pt was evaporated from Pt slug (99.99% purity) using an e-beam evaporator with a current of 130 mA and a voltage of 9 kV at a pressure of 1×10^{-6} mbar. (Electron-beam evaporation)	S8
Cu/Pt Micromotors	electrochemical deposition	A layer of copper is deposited on top of the polycarbonate template, and the Pt segment was electrodeposited subsequently at -2 mA for 600 s (Autolab type III electrochemical analyzer)	S9
MIMS/Pt Janus Micromotors	sputtering method	A single layer of magnetic illite microspheres (MIMSs) was tiled on the slide, and Pt was sputtered in the direction vertical to the glass slide (Mini-sputter, MCM-100P, SEC, South Korea)	S10

References

S1. W. J. Chun, A. Ishikawa, H. Fujisawa, T. Takata, J. N. Kondo, M. Hara, M. Kawai, Y. Matsumoto and K. Domen, Conduction and valence band positions of Ta_2O_5, TaON, and Ta_3N_5 by UPS and electrochemical methods, *J. Phys. Chem. B*, 2003, **107**, 1798-1803.

S2. T. S. Tofa, F. Ye, K. L. Kunjali and J. Dutta, Enhanced visible light photodegradation of microplastic fragments with plasmonic platinum/zinc oxide nanorod photocatalysts, *Catalysts*, 2019, **9**, 819.

S3. A. M. Pourrahimi, K. Villa, C. L. Manzanares Palenzuela, Y. Ying, Z. Sofer and M. Pumera, Catalytic and light-driven ZnO/Pt janus nano/micromotors: switching of motion mechanism via interface roughness and defect tailoring at the nanoscale, *Adv. Funct. Mater.*, 2019, **29**, 1808678.

S4. J. Hwang, H. M. Yang, K. W. Lee, Y. I. Jung, K. J. Lee and C. W. Park, A remotely steerable Janus micromotor adsorbent for the active remediation of Cs-contaminated water, *J. Hazard. Mater.*, 2019, **369**, 416-422.

S5. C. M. Oral, M. Ussia, D. K. Yavuz and M. Pumera, Shape Engineering of TiO_2 Microrobots for "On-the-Fly" Optical Brake, *Small*, 2022, **18**, 2106271.

S6. Z. Xiao, S. Duan, P. Xu, J. Cui, H. Zhang and W. Wang, Synergistic speed enhancement of an electric-photochemical hybrid micromotor by tilt rectification, *ACS Nano*, 2020, **14**, 8658-8667.

S7. X. Lyu, X. Liu, C. Zhou, S. Duan, P. Xu, J. Dai, X. Chen, Y. Peng, D. Cui, J. Tang, X. Ma, and W. Wang, Active, yet little mobility: Asymmetric decomposition of H_2O_2 is not sufficient in propelling catalytic micromotors, *J. Am. Chem. Soc.*, 2021, **143**, 12154-12164.

S8. A. M. Pourrahimi, K. Villa, Y. Ying, Z. Sofer and M. Pumera, ZnO/ZnO_2/Pt Janus micromotors propulsion mode changes with size and interface structure: enhanced nitroaromatic explosives degradation under visible light, *ACS Appl. Mater. Interfaces*, 2018, **10**, 42688-42697.

S9. J. G. S. Moo, S. Presolski and M. Pumera, Photochromic spatiotemporal control of bubble-propelled micromotors by a spiropyran molecular switch, *ACS Nano*, 2016,

10, 3543-3552.

S10. C. W. Park, T. Kim, H. M. Yang, Y. Lee and H. J. Kim, Active and selective removal of Cs from contaminated water by self-propelled magnetic illite microspheres, *J. Hazard. Mater.*, 2021, **416**, 126226.